SUPPLEMENTARY FIGURES

Supplementary Figure S1.

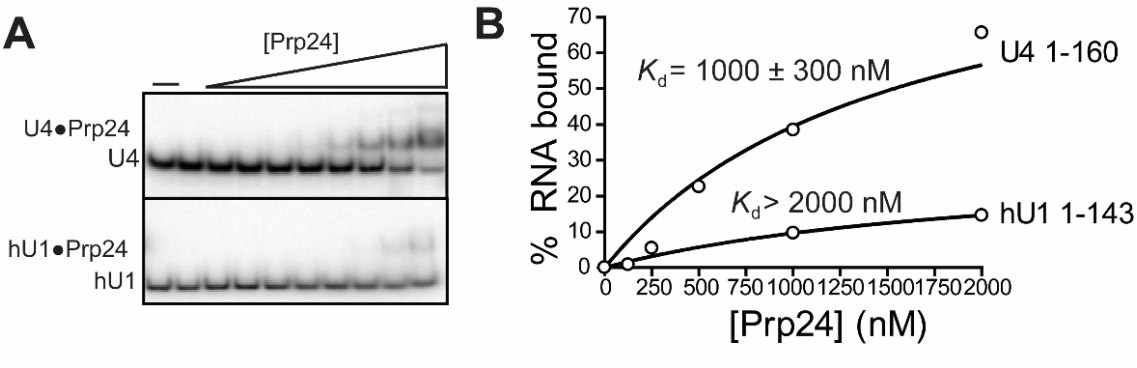

Supplementary Figure S1. Prp24 binds U4 with greater affinity than a control RNA of similar length. A) Native gel analysis comparing Prp24 binding to U4 RNA (top) and a non-specific control, human U1 RNA (bottom). B) Quantitation of Prp24 binding to U4 and hU1 RNAs. Prp24 binds U4 with a K_d of 1000 nM, while the binding of Prp24 to hU1 is significantly weaker and cannot be accurately quantified.

Supplementary Figure S2.

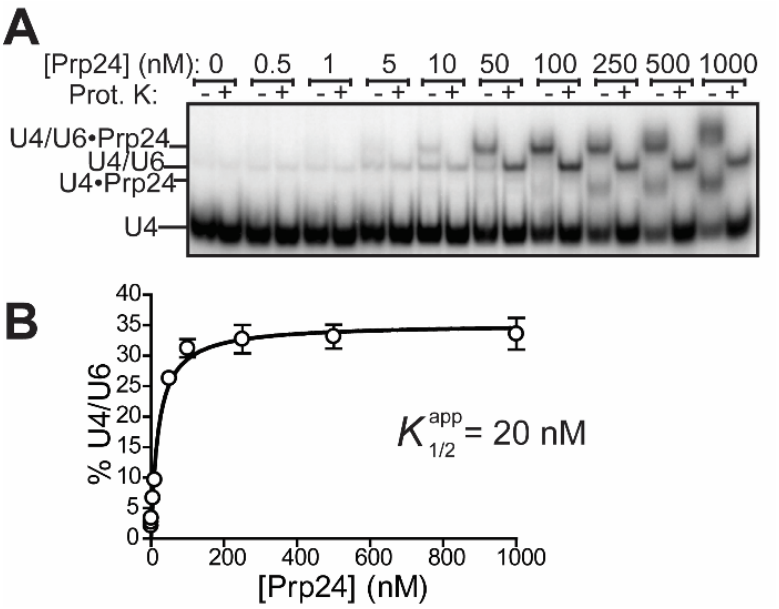

Supplementary Figure S2. Effect of Prp24 concentration on the rate of annealing. A) Native gel showing the formation of U4/U6 at a single time point (90 minutes) in the presence of increasing concentrations of full-length Prp24. Samples were divided into intact ribonucleoprotein (minus lanes) and proteinase K-treated (plus lanes) samples. B) Quantification of U4/U6 formation after 90 minutes for varying concentrations of Prp24.

Supplementary Figure S3.

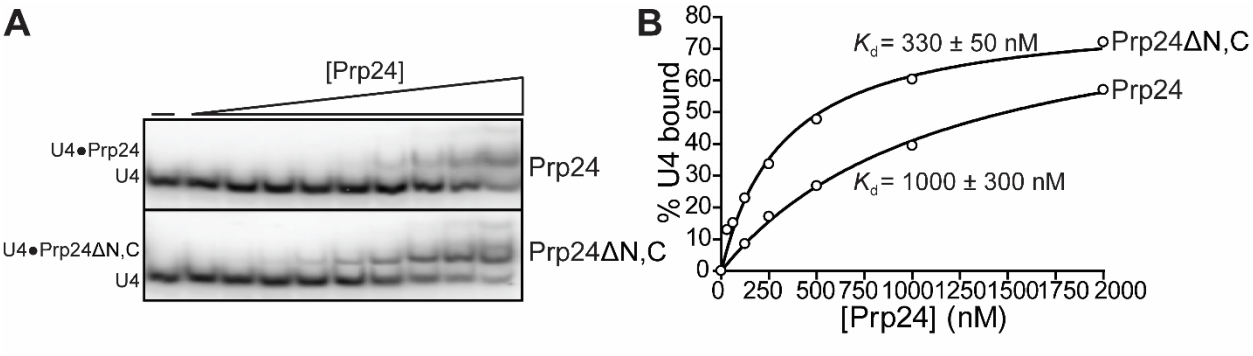

Supplementary Figure S3. Truncation of Prp24 protein enhances binding to U4 RNA. A) Native gel analysis of U4-Prp24 binding. Full-length Prp24 (top) and truncated Prp24 (bottom) both bind U4 RNA. B) Truncated Prp24 (ΔN,C) binds U4 with a K_d of 320 nM, while full-length Prp24 binds with a K_d of 1000 nM.

Supplementary Figure S4.

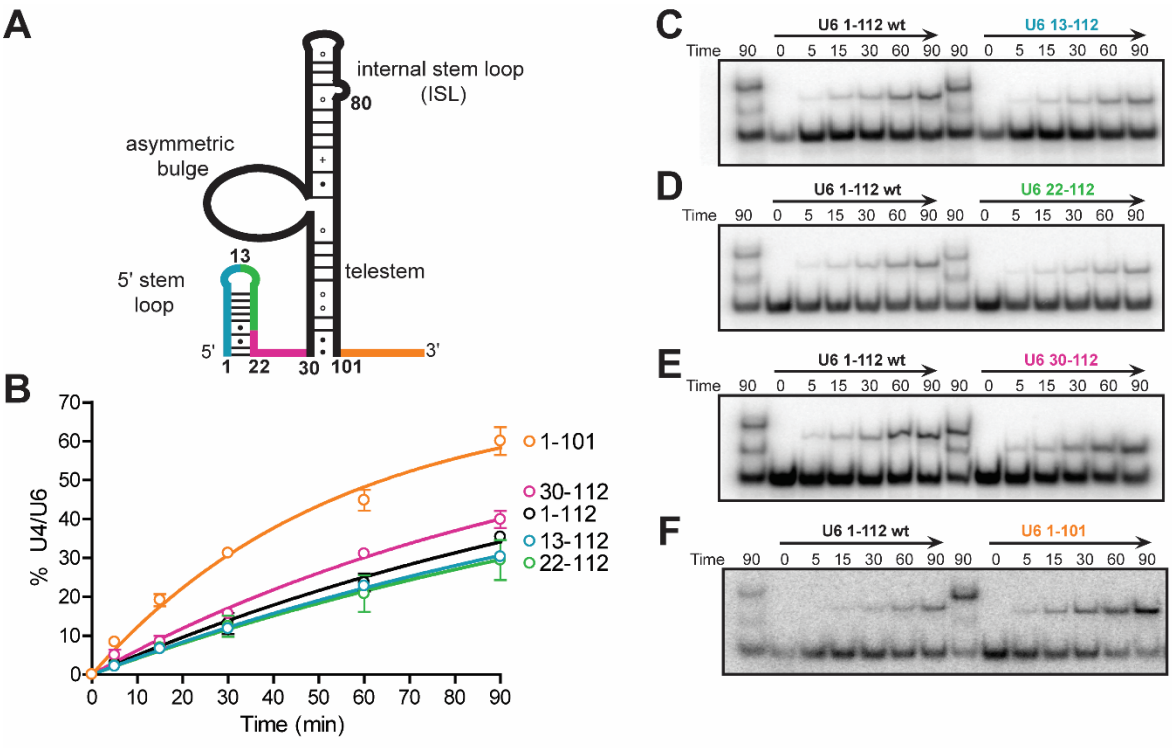

Supplementary Figure S4. Truncation of U6 RNA does not impede U4/U6 annealing. A) Secondary structure of U6 showing the regions deleted. B) Quantification of annealing rates for truncations of U6. C-F) Annealing gels comparing wild-type U6 to various truncations of U6. In all gels, a control lane containing the annealing reaction at 90 minutes that has not been proteinase K-treated precedes a time course of annealing reactions treated with proteinase K. C) Truncation of U6 to nucleotides 13-112, disrupting the 5' stem-loop. D) Truncation of U6 to nucleotides 22-112, removing the 5' stem-loop. E) Truncation of U6 to nucleotides 30-112, removing the 5' stem-loop and linker region. F) Truncation of U6 to nucleotides 1-101, removing the 3' single stranded region.

Supplementary Figure S5.

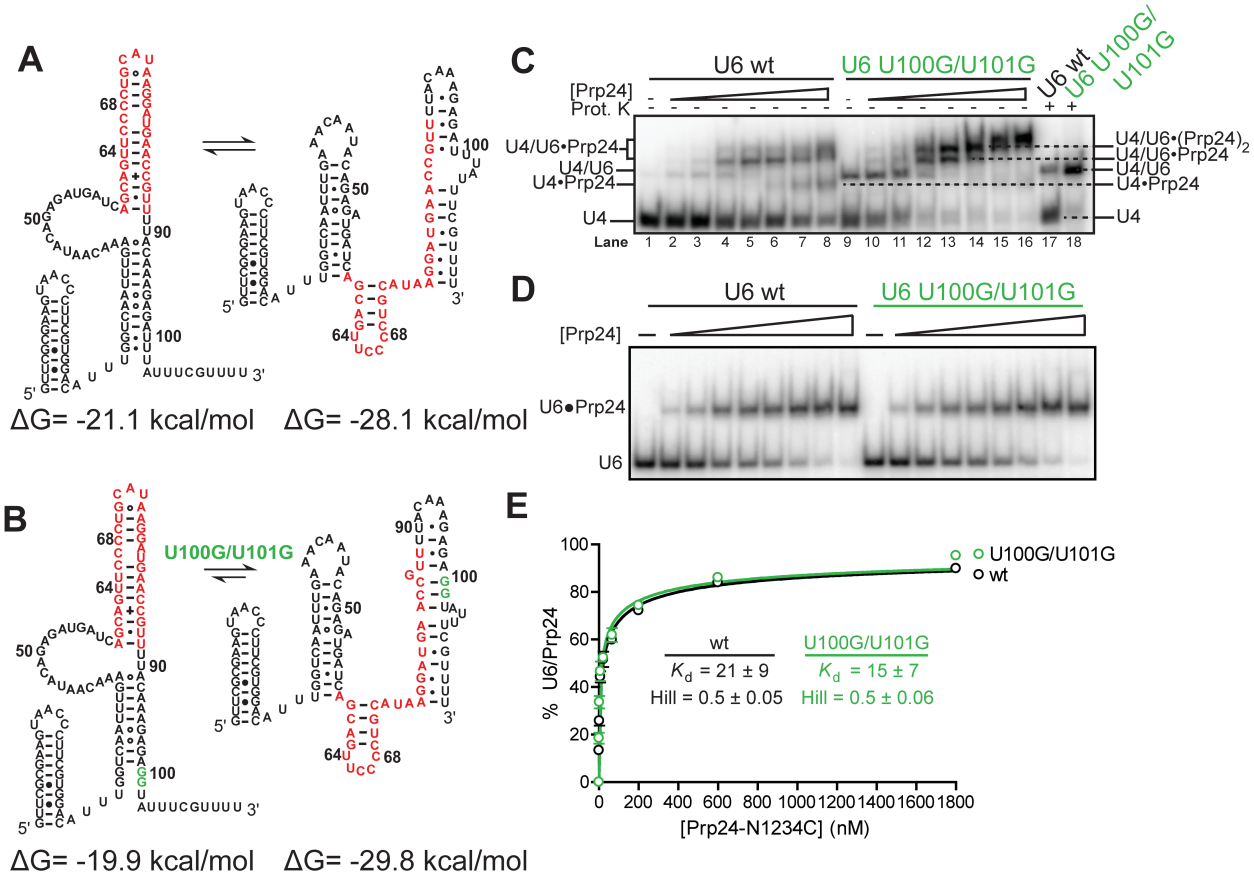

Supplementary Figure S5. A) Secondary structure of wild-type RNA (left) is predicted to be in equilibrium with a more stable alternative secondary structure in the absence of Prp24. MFold predicted free energies are indicated below secondary structures. The ISL region is shown in red. B) The U100G/U101G mutations are predicted to further stabilize the putative alternative fold, which may account for the observed protein-free annealing rates. C) Titration of Prp24 reveals multiple binding sites on U4/U6-U100G/U101G (mutant #4). U4 and U6 (wt vs. U100G/U101G) were incubated for 90 minutes with increasing concentrations of Prp24. In lanes 17 and 18, 250 nM Prp24 was incubated with U4 and U6 for 90 minutes and then Proteinase K treated. D) Native gel analysis of U6-Prp24 binding comparing wild type (left) and U6-U100G/U101G (right). E) Prp24-binding curves of wild-type and mutant U6 RNA.

Supplementary Figure S6.

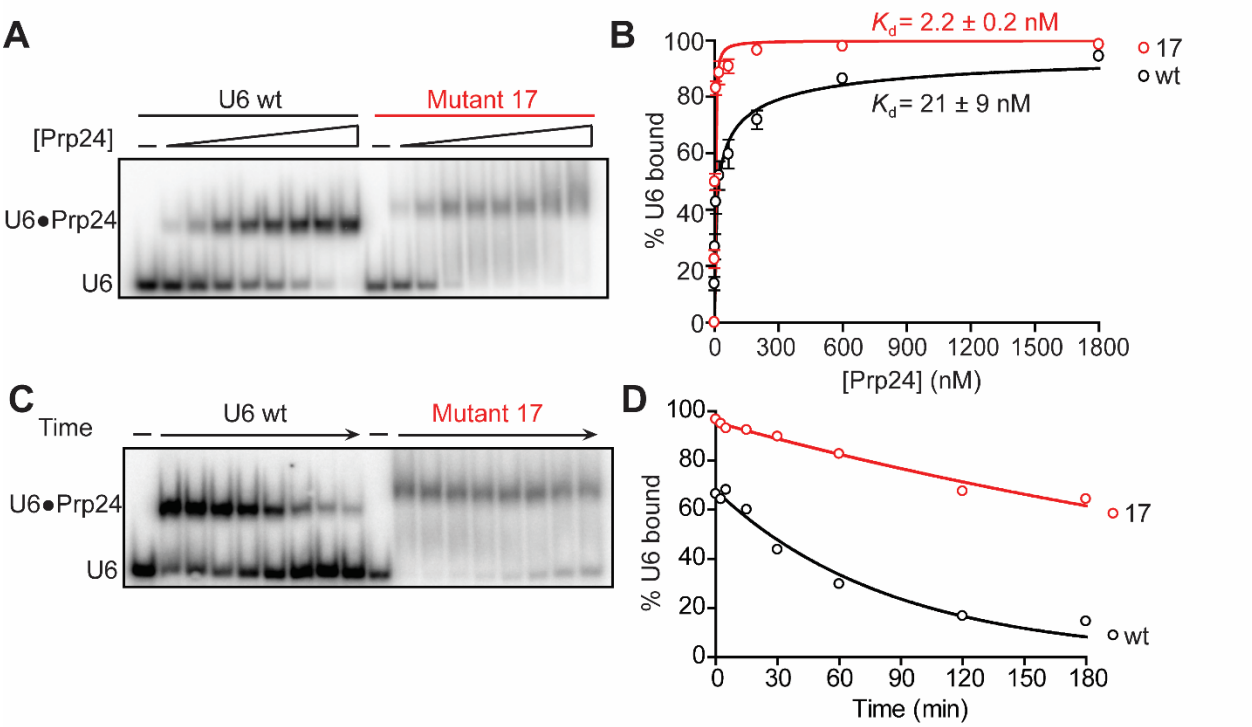

Supplementary Figure S6. Hyperstabilization of the telestem strengthens U6-Prp24 binding. A) Native gel analysis of U6-Prp24 binding for wild-type (left) and mutant 17 (right) RNAs. B) Binding curves of wild-type and mutant RNA. C) Native gel analysis of off-rates for wild-type and mutant RNA. Radiolabeled U6-Prp24 was formed with 50 nM Prp24, then challenged with 200 nM unlabeled U6 (a > 200-fold excess) for increasing lengths of time. D) Quantification of off-rate gel. Data was fit with a one phase exponential decay equation.

Supplementary Figure S7.

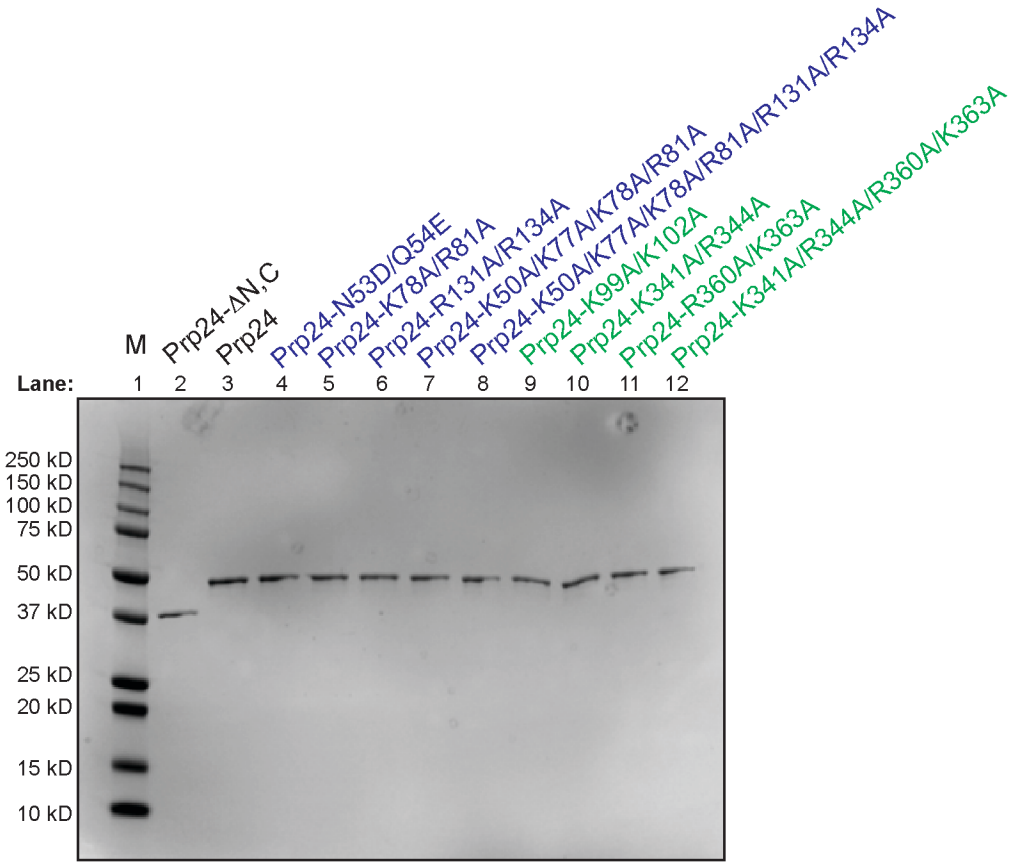

Supplementary Figure S7. SDS-PAGE gel of purified recombinant Prp24 constructs.